

RESEARCH ARTICLE

Lunge filter feeding biomechanics constrain rorqual foraging ecology across scale

S. R. Kahane-Rapport^{1,*}, M. S. Savoca¹, D. E. Cade^{1,2}, P. S. Segre¹, K. C. Bierlich³, J. Calambokidis⁴, J. Dale³, J. A. Fahlbusch¹, A. S. Friedlaender², D. W. Johnston³, A. J. Werth⁵ and J. A. Goldbogen¹

ABSTRACT

Fundamental scaling relationships influence the physiology of vital rates, which in turn shape the ecology and evolution of organisms. For diving mammals, benefits conferred by large body size include reduced transport costs and enhanced breath-holding capacity, thereby increasing overall foraging efficiency. Rorqual whales feed by engulfing a large mass of prey-laden water at high speed and filtering it through baleen plates. However, as engulfment capacity increases with body length (engulfment volume \propto body length^{3.57}), the surface area of the baleen filter does not increase proportionally (baleen area \propto body length^{1.82}), and thus the filtration time of larger rorquals predictably increases as the baleen surface area must filter a disproportionately large amount of water. We predicted that filtration time should scale with body length to the power of 1.75 (filter time \propto body length^{1.75}). We tested this hypothesis on four rorqual species using multi-sensor tags with corresponding unoccupied aircraft systems-based body length estimates. We found that filter time scales with body length to the power of 1.79 (95% CI: 1.61–1.97). This result highlights a scale-dependent trade-off between engulfment capacity and baleen area that creates a biomechanical constraint to foraging through increased filtration time. Consequently, larger whales must target high-density prey patches commensurate to the gulp size to meet their increased energetic demands. If these optimal patches are absent, larger rorquals may experience reduced foraging efficiency compared with smaller whales if they do not match their engulfment capacity to the size of targeted prey aggregations.

KEY WORDS: Filtration, Scaling, Baleen whale, Constraints

INTRODUCTION

Body size influences the evolution of morphological traits and physiological performance (Alexander, 1998; Hespeneide, 1973; Schmidt-Nielsen, 1984). Regardless of taxa, large body size is generally thought to confer a wide range of physiological and ecological benefits (Calder, 1984; Peters, 1983; Slater et al., 2017). However, large body size can have myriad consequences on structure and function because of the fundamental principles of

morphological scaling (Haldane, 1926), resulting in functional trade-offs that ultimately impact evolution and ecology.


The physiological advantages and disadvantages associated with different body sizes have wide-ranging effects, from behavior to life history. For example, the smallest animals have the lowest absolute energetic demands (Kelt and Van Vuren, 1999), yet they may also struggle with thermoregulation and be forced to compensate by increasing their metabolism (Scholander et al., 1950; Taylor et al., 1980). Small size enables high performance maneuverability and agility (Domenici, 2001), but may limit maximum attainable speeds (Carrier, 1994; Hirt et al., 2017). Conversely, larger animals may retain heat more easily (Irving, 1973) and exhibit lower mass-specific metabolic rates (Paladino et al., 1990; White and Kearney, 2014) but require greater absolute energy intake (Peters, 1993). Although evolution trends towards increasing body size within species lineages, extinction disproportionately affects animals of large body size, in part because of their dependence on a stable environment (Clauset, 2013; Friedman et al., 2010; Holliday, 2005; Smith et al., 2018).

Despite the high extinction risk, extremely large size (gigantism) has evolved many times, particularly in the oceans (Clauset, 2013; Vermeij, 2016). The largest marine animals of both the past and present tend to be filter feeders (Friedman et al., 2010). Although aquatic filter feeding has evolved in many diverse invertebrate and vertebrate lineages, different modes of filtration (active, passive) among this feeding guild reflect functional constraints associated with body size. Filter feeders face the unique challenge of ensuring that their filter apparatus is sufficiently large to catch prey to support the cost of increasing body size (Sebens, 1982). For example, passive filter feeders, such as sponges and bivalves, rely on water flow to carry particles to their feeding structures (LaBarbera, 1984). In contrast, active filter feeders, such as baleen whales (suborder: Mysticeti), use swimming-induced pressures to drive water through an engulfment apparatus and oral filter (Goldbogen et al., 2017). Among mysticetes, this feeding style has further diversified: balaenid whales are ram filter feeders, while balaenopterid whales, also known as ‘rorqual whales’, are lunge filter feeders. Some species of rorqual whales, such as blue whales (*Balaenoptera musculus*) and fin whales (*Balaenoptera physalus*), rank among the largest animals of all time. The combination of extreme size and filter feeding may pose unexplored constraints and benefits to foraging performance.

Gigantic body sizes in mysticetes (>15 m in body length) evolved in conjunction with the baleen filter feeding mechanism relatively recently, less than 5 million years ago (Slater et al., 2017). The unique rorqual filter feeding strategy involves the intermittent engulfment of a large prey-laden mass of water that is subsequently filtered through baleen plates that occupy a narrow space between the nearly closed jaws (Werth, 2000). In some large rorqual species, the engulfed water mass is greater than that of their own body (Kahane-Rapport and Goldbogen, 2018). As a result, this lunge feeding mechanism carries a high energetic cost, owing to high

¹Department of Biology, Hopkins Marine Station, Stanford University, Pacific Grove, CA 93950, USA. ²Institute of Marine Sciences, University of California, Santa Cruz, Santa Cruz, CA, USA. ³Nicholas School of the Environment, Duke University Marine Laboratory, Beaufort, NC 27710, USA. ⁴Cascadia Research Collective, 218 W. 4th Ave., Olympia, WA 98501, USA. ⁵Department of Biology, Hampden-Sydney College, Hampden-Sydney, VA 23943, USA.

*Author for correspondence (skahaner@stanford.edu)

 S.R.K., 0000-0002-5208-1100; M.S.S., 0000-0002-7318-4977; D.E.C., 0000-0002-1080-0250; P.S.S., 0000-0002-2396-2670; K.C.B., 0000-0001-9724-6055; J.C., 0000-0002-5028-7172; J.A.F., 0000-0001-9275-013X; A.S.F., 0000-0002-2822-233X; D.W.J., 0000-0003-2424-036X; J.A.G., 0000-0002-4170-7294

drag, but provides the animal with extraordinary engulfment capacity (Goldbogen et al., 2007). Filtering large quantities of water is energetically efficient when foraging on dense patches of krill (Goldbogen et al., 2019). High-density krill patches are frequently found relatively deep in the ocean (Friedlaender et al., 2019; Goldbogen et al., 2011), so air-breathing filter feeders must dive to achieve the energetic efficiency needed to power daily activities and for the long-distance migration to breeding grounds (Potvin et al., 2012; Wiedenmann et al., 2011).

For aquatic lineages that push the physiological and biomechanical limits of size and the evolution of complex filter feeding mechanisms, it is unclear how these features affect performance and ecological niche at the upper extreme of body mass (BM). Rorqual foraging performance is a balance between minimizing oxygen use and maximizing energy intake during a foraging dive. In particular, gigantic rorquals likely face functional trade-offs associated with their filter feeding mechanism as well as the conflicting demands of high-cost foraging during breath-hold dives. Here, we examine the scaling of rorqual feeding morphology and predict how body size both enhances and constrains foraging performance.

Scaling hypothesis for rorqual filter time

Isometric scaling theory predicts that a volume, such as the engulfment capacity, should scale with body length (BL) in proportion to BL^3 , and that an area, such as the baleen area, should scale in proportion to BL^2 [first principles as described by Galileo Galilei in 1638, translated into English (Galilei, 1914)]. Filter time is determined by how long it takes the volume of water within the feeding pouch to be purged through the area that the baleen plates occupy in the mouth:

$$\text{Filter time} = \frac{\text{Engulfment volume}}{\text{Baleen area} \times \text{Flow speed}}, \quad (1)$$

$$\text{Filter time} \propto \frac{\text{Engulfment volume} \propto BL^3}{(\text{Baleen area} \propto BL^2) \times (\text{Flow speed} \propto BL^0)}. \quad (2)$$

Therefore, filter time is predicted to be proportional to BL^1 . We assumed flow speed and pressure drop were invariant across body size because the spacing of the baleen plates (~ 1 cm between each plate) is consistent across all rorqual species (Werth et al., 2018).

However, Kahane-Rapport and Goldbogen (2018) calculated engulfment capacity of rorqual whales using a two-quarter ellipsoid model of the mouth (further detailed in Goldbogen et al., 2010), and found that engulfment capacity exhibits positive allometry within and across rorqual species (across species: engulfment capacity $\propto BL^{3.57}$) (Fig. 1); larger whales have relatively larger engulfment capacities compared with smaller whales. In contrast, Werth et al. (2018) found that baleen area exhibits negative allometry within and across rorqual species (across species: baleen area $\propto BL^{1.82}$) (Fig. 1). Werth et al. (2018) followed Kawamura (1974), using a 2D model to calculate baleen area (Kawamura, 1974). This 2D model calculated the inner (medial) surface of each rack by finding the area of a curved arch-like shape, and assumed this shape represents the filter ‘window’ through which the engulfed water must be purged during the filtration phase.

Using our knowledge of how the scaling of engulfment volume and baleen area diverge from isometry, we can reassess our prediction of how filter time scales in proportion to BL. Engulfment volume scales in proportion to BL with an exponent of 3.57, and baleen area scales in proportion to BL with an exponent of 1.82. Thus, filter time

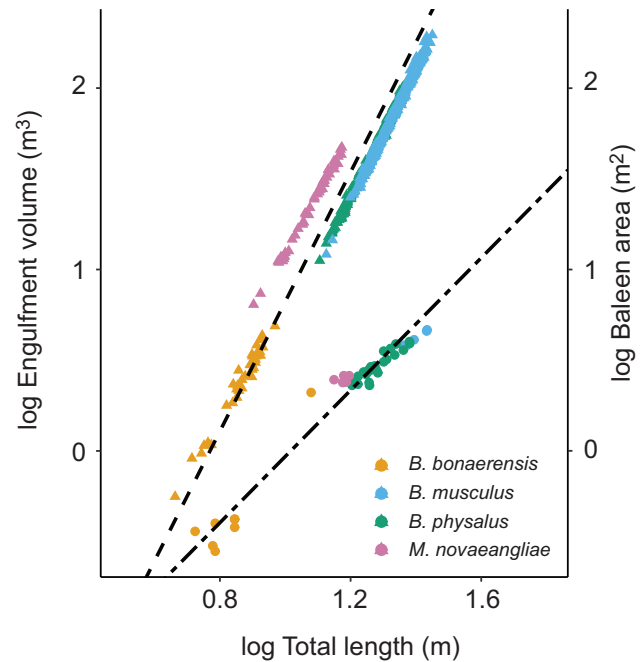


Fig. 1. Scaling of engulfment capacity volume (Kahane-Rapport and Goldbogen, 2018) and baleen area (Werth et al., 2018) in four rorqual species (blue whale, *Balaenoptera musculus*; fin whale, *Balaenoptera physalus*; humpback whale, *Megaptera novaeangliae*; Antarctic minke whale, *Balaenoptera bonaerensis*). Each point represents an individual whale; data from 33 minke whales, 489 blue whales, 491 fin whales and 51 humpback whales were used for engulfment volume calculations and data from eight minke whales, five blue whales, 30 fin whales and eight humpback whales were used for baleen area calculations. The dashed line represents the linear regression for engulfment capacity volume (slope=3.57; intercept=-2.75, CI: 3.56–3.58) and the dot-dash line represents the linear regression for baleen area (slope=1.82; intercept=-1.855; CI: 1.71–1.939).

scales in proportion to BL with an exponent of 1.75:

$$\text{Filter time} \propto \frac{\text{Engulfment volume} \propto BL^{3.57}}{(\text{Baleen area} \propto BL^{1.82}) \times (\text{Flow speed} \propto BL^0)} \quad (3)$$

$$\text{Filter time} \propto BL^{1.75}. \quad (4)$$

These data suggest that the differential scaling of baleen area and engulfment capacity acts as a fundamental biomechanical constraint to performance, which will be reflected in rorqual foraging behavior as a decrease in lunge feeding events. The positive allometry of engulfment capacity suggests that the cost of lunge feeding also exhibits positive allometry, and thus will progressively limit dive time (Goldbogen et al., 2012). In conjunction with an oxygen limit and a high-cost maneuver, it becomes increasingly important for animals of disproportionately large engulfment volumes to ensure that each lunge target high-density prey. Time and energy spent filtering out a lunge with a sub-optimal prey density will create the greatest burden on those rorquals whose lengthy filter time delays their ability to find a better patch, which we interpret as an ecological constraint. Here, we provide an empirical test of this prediction using tag-based measurements of filter time and drone-based measurements of BL to determine feeding performance and filter time as a function of body size.

MATERIALS AND METHODS

Morphological measures

The engulfment capacity estimates in Fig. 1 are from Kahane-Rapport and Goldbogen (2018) and are summarized here. These engulfment capacity estimates are derived from the Discovery Reports that contain morphological data for 33 Antarctic minke whales (*Balaenoptera bonaerensis*), 489 blue whales (*Balaenoptera musculus*), 491 fin whales (*Balaenoptera physalus*) and 51 humpback whales (*Megaptera novaeangliae*) (Mackintosh, 1929, 1942; Matthews, 1937, 1938). Baleen area calculations for eight minke whales, five blue whales, 30 fin whales and eight humpback whales were taken from Werth et al. (2018) (Fig. 1). Werth et al. (2018) followed Kawamura (1974), using a 2D model to calculate baleen area. Werth et al. (2018) also provided total BL measures for each of the whales. We estimated filter time using these data as described in Eqns 3 and 4.

Filtration rate calculations: tag data

We used motion-sensing suction-cup attached tags (Customized Animal Tracking Solutions, www.cats.is) to collect high sample rate kinematic and behavioral data from 21 blue whales (Monterey Bay), three fin whales (Eastern Greenland and Monterey Bay), nine humpback whales (Antarctic Peninsula and Monterey Bay) and nine Antarctic minke whales (Antarctic Peninsula) between 2017 and 2019. All tagging work was performed under permit from the National Marine Fisheries Service (nos. 16111 and 21678), Administrative Panel on Laboratory Animal Care (no. 30123) and National Oceanic and Atmospheric Administration Office of National Marine Sanctuaries Multiple Sanctuary Permit (permit no. MULTI-2019-009).

For all tag deployments, accelerometers (dynamic range $\pm 39.2 \text{ m s}^{-2}$) were sampled at 400 Hz, magnetometers and gyroscopes (dynamic range 1000 deg s^{-1}) were sampled at 50 Hz, and pressure was sampled at 10 Hz. All data were decimated to 10 Hz before further analysis. Tag orientation was corrected to whale-frame using periods of known orientation, and animal orientation (pitch, roll and heading) was calculated using custom-written MATLAB scripts (Cade et al., 2016; Johnson and Tyack, 2003). Continuous animal speed was determined using the amplitude of tag vibrations (Cade et al., 2018). Video and sound were recorded concurrently and were aligned with sensor data by the MATLAB script (Cade et al., 2016).

We visualized the kinematic record to identify lunge feeding events (Fig. 2). Lunges have a distinct kinematic signature, similar across all species of rorquals. A lunge is confirmed by (1) fluking associated with a distinct speed maximum and (2) rapid deceleration with some continued forward momentum, owing to the engulfed water mass (Goldbogen et al., 2017). After the lunge was determined, we marked mouth opening at the peak in speed, and mouth closing as the point after the sharpest deceleration in speed and as the beginning of the filtration phase (Cade et al., 2016). At mouth close, the ventral groove blubber contains the engulfed water mass, the mass of which slows the forward momentum of the rorqual (Potvin et al., 2009; Simon et al., 2012). This rapid deceleration and subsequent gliding period are visible in the kinematic record. Once the water has been filtered from the pouch, the whale begins fluking and accelerates to prepare for another lunge, or begins ascending to the surface. We marked this point in the kinematic record as the cessation of filtration.

We verified that filtration was occurring during these gliding periods from whale-borne tag video. By using four blue whale video tag deployments, in which the entire engulfment to end of filtration

sequence was visible, we determined that blue whale average filter time was $53.84 \pm 4.84 \text{ s}$ (mean \pm s.d.). By using two minke whale video tag deployments, in which the entire engulfment to end of filtration sequence was visible, we determined that average filter time was $8.35 \pm 1.29 \text{ s}$ (mean \pm s.d.). Thus, we are confident that the kinematic signatures used to identify filter time are accurate because the filter time results from kinematic data alone fall within the range of visually verified filter time. Additionally, dive duration was determined by identifying the elapsed time between surfacing events that were separated by a dive to a depth greater than 50 m with at least one lunge. We only analyzed dives that exceeded 50 m as behavior close to the surface is not constrained by oxygen and to avoid kinematic data associated with surfacing.

Body size measurements: unoccupied aircraft systems data

We collected high-resolution aerial images using unoccupied aircraft systems (UAS) from 2017 to 2019. Each of the aforementioned tagged whales has a high-resolution image taken around the time of tag deployment.

We used a DJI Phantom 3 Professional quadcopter, a DJI Phantom 4 Pro quadcopter and two types of hexacopters, the FreeFly Alta6 and a custom Mikrokopter-based LemHex-44, to collect drone imagery. The Phantom 3 Professional quadcopter was fitted with a Sony EXMOR 1/2.3" camera, 4000×3000 pixel resolution and a 94 deg field of view. The Phantom 4 Pro quadcopter was fitted with a 1" CMOS camera sensor, 5472×3078 pixel resolution and an 84 deg field of view. Both hexacopters were fitted with a Lightware SF11/C laser altimeter and a Sony Alpha A5100 camera with an APS-C ($23.5 \times 15.6 \text{ mm}$) sensor, 6000×4000 pixel resolution, and either a Sony SEL 50 mm or SEL 35 mm focal length low distortion lens. The laser altimeter and cameras were co-located on a two-axis gimbal with pitch angle controlled via remote control to aid in positioning and ensure image collection at nadir. Measurement errors for all aircraft were calculated by measuring a known sized frame floating at the surface from various altitudes. All aircraft had an average measurement error of $<5\%$. We used similar methods for hand launch and recovery from small boats as described in Durban et al. (2016), with the addition of a first-person view (FPV) screen attached to each flight controller, giving the pilot a live feed from the photogrammetry camera. The LemHex-44 required a single operating pilot, who manually controlled the gimbal and camera's shutter, whereas the Alta6 required two operators, a pilot and camera operator. We collected images in bursts with a high shutter rate of 6 frames s^{-1} (LemHex-44 and Alta6) or on a 2 s timer (Phantom 3, Phantom 4). Measurements were made using MorphoMetriX on images with the whale in full frame lengthwise and as the animal surfaced or was just below the surface (Torres and Bierlich, 2020). Measurement outputs from MorphoMetriX were collated using CollatriX (Bird and Bierlich, 2020).

Water processed calculation

We determined how much water a whale processed per dive in both absolute and mass-specific terms. As we had BL for each tagged whale, we estimated engulfment capacity (Goldbogen et al., 2011; Kahane-Rapport and Goldbogen, 2018) and multiplied that capacity by the number of lunges performed in a given dive to determine total water engulfed per dive. Additionally, we estimated mass using the allometric equations detailed in Kahane-Rapport and Goldbogen (2018) to calculate mass-specific engulfment capacity per dive to determine how the mass-specific cost of foraging affects lunge count.

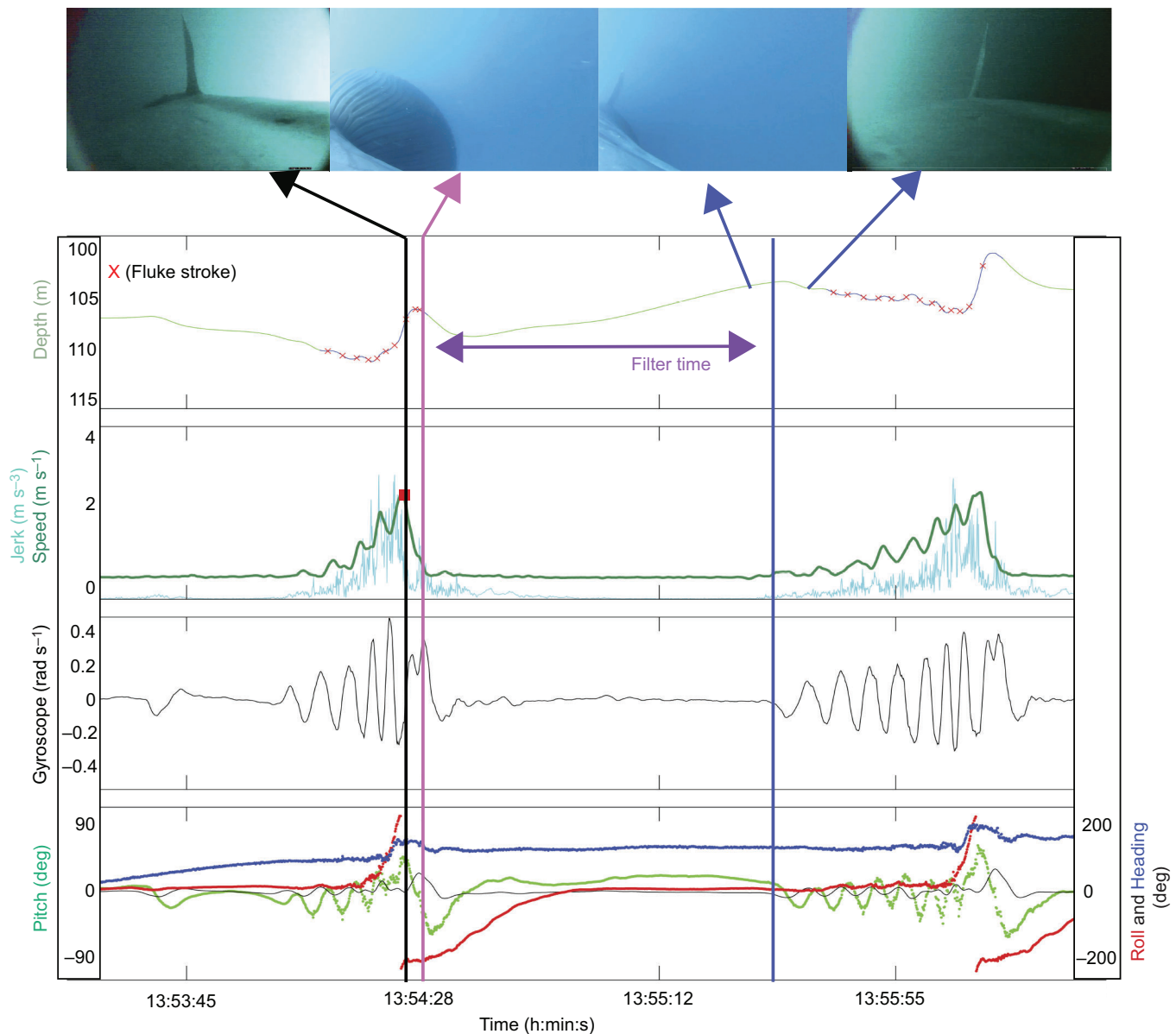


Fig. 2. Example kinematic signatures used to identify filter time from a blue whale deployment. The lunge is marked by the red square, the vertical black line represents mouth opening, the vertical pink line represents mouth closure, and the vertical blue line represents the end of filtration. Images above are from a tagged blue whale, showing whale behavior aligned with the concurrent kinematics.

Statistical analyses to estimate filter time

To test whether the scaling relationship of engulfment capacity and baleen area (i.e. ‘calculated data’, see Eqns 3 and 4) robustly estimates filter time measured from tag data, we used a Bayesian generalized linear mixed model (GLMM), using the MCMCglmm package (Hadfield, 2010) in R (<https://www.r-project.org/>). For this model, we used UAS-measured BL to predict tag-measured filter time with a random effect of individual to control for pseudoreplication. We expected that the 95% confidence interval of the slope from the relationship of total length to filter time, as modeled using the MCMCglmm, would encompass the value predicted by the calculated data (1.75).

To model the relationship between dive duration and body mass, we used a GLMM. We used UAS-measured BL to predict tag-measured dive duration. To test the relationship between the volume of engulfed water and BL, we used a GLMM and used UAS-measured BL to

predict modeled engulfment capacity. To test the relationship between the mass-specific engulfment capacity and BL, we used a GLMM. We used UAS-measured BL to predict mass-specific engulfment capacity. Each model had a random effect of individual to control for pseudoreplication. All models were fit with the lme4 package (Bates et al., 2015) in R (<https://www.r-project.org/>). All variables were \log_{10} transformed, which is standard practice for investigating ecological scaling relationships (Kerkhoff and Enquist, 2009).

To determine how lunge count per dive relates to BL and mean depth, we used a GLMM with a Poisson distribution with a random effect of individual, using the lme4 package (Bates et al., 2015) in R (<https://www.r-project.org/>).

RESULTS

Based on analyses of tag kinematic data, we used 3116 blue whale lunges, 577 fin whale lunges, 788 humpback lunges and 2578

Table 1. Average filter time (s) varied by species

Species	<i>n</i>	Mean (s)	s.d.
Minke	9	8.88	6.09
Humpback	8	17.12	5.95
Fin	3	31.30	11.56
Blue	21	60.27	20.36

minke whale lunges to determine filter time for each species (Table S1). Average filter time for blue whales was 60.27 ± 20.36 s, 31.3 ± 11.56 s for fin whales, 17.12 ± 5.95 s for humpback whales and 8.88 ± 6.09 s for minke whales (mean \pm s.d.; Table 1). Minke whales averaged 7.48 ± 0.14 lunges per dive, humpback whales 6.28 ± 0.37 , fin whales 3.95 ± 0.13 and blue whales 4.02 ± 0.05 , during dives at depths >50 m (mean \pm s.e.m.; Table 2). During a foraging dive, minke whales spent $21.43 \pm 8.482\%$ of their dive time filtering, humpback whales $26.845 \pm 9.106\%$, fin whales $29.630 \pm 10.561\%$ and blue whales $40.832 \pm 11.826\%$ (mean \pm s.d.; Table S2).

The scaling of the calculated morphological data predicted the scaling of foraging behavior from tag data across the species of rorquals in this study. The empirical relationship between filter time and body size had a slope of 1.79; the confidence interval for this value (95% CI: 1.61–1.97) encompassed our predicted slope from the calculated data (i.e. the engulfment capacity and baleen area) of 1.75 (Fig. 3).

When controlling for depth, we found that animals of greater BL lunged less per dive. Using a GLMM, we demonstrate that for all species, the effect of dive depth on lunge count is positive, meaning that lunge count increases with increasing depth (Poisson GLMM, $z_{40,1313} = 8.821$, $P < 0.0001$). We also found that the effect of BL is negative, meaning that lunge count decreases with increasing BL (Poisson GLMM, $z_{40,1313} = -7.056$, $P < 0.00001$).

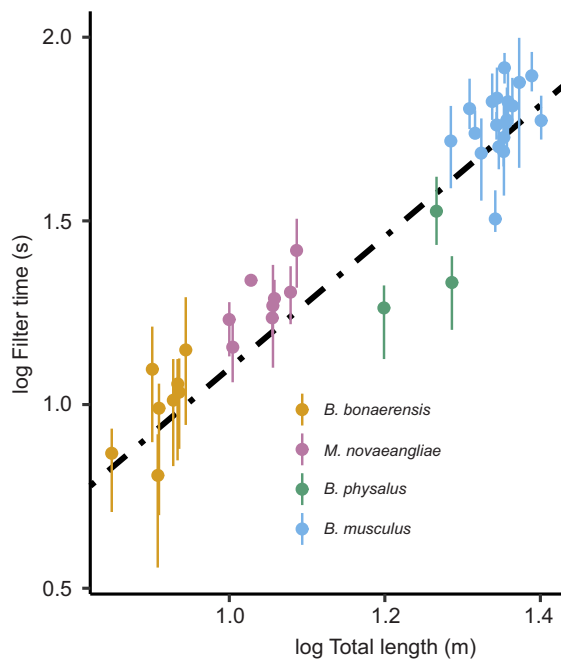


Fig. 3. Scaling of mean filter time (s) in four rorqual species as a function of total body length (m) measured using unoccupied aircraft systems (UAS) imagery. Nine minke whale deployments, three fin whale deployments, 21 blue whale deployments and eight humpback whale deployments were used in this analysis. Bars on each point represent interquartile range (25–75%). Dashed line represents a general linear mixed model (slope=1.79; intercept=-0.692; CI: 1.61–1.97).

Table 2. Average, median and maximum number of lunges per dive deeper than 50 m, varied by species

Species	<i>n</i>	Mean	Median	s.e.m.	s.d.	Maximum
Minke	9	7.48	7.0	0.14	2.53	18
Humpback	8	6.28	5.0	0.37	3.99	16
Fin	3	3.95	4.0	0.13	1.60	9
Blue	21	4.02	4.0	0.05	1.47	11

Further, using a GLMM, we found that the relationship between dive duration and BM across all species had a slope of 0.38 (95% CI 0.33–0.42) (Fig. 4). Large whales engulf more water, in both relative and absolute terms. Using a GLMM, we found that the relationship between water engulfed per dive and BL across species had a slope of 3.35 (95% CI 3.17–3.52). We also used a GLMM to show that the relationship between mass-specific water engulfed per dive and BL across all species had a slope of 1.10 (95% CI: 1.08–1.13) (Fig. 5).

DISCUSSION

The aim of our study was to understand the filtration rate of rorquals across species of different body size. We predicted filtration rate in these animals using two different methods: (1) scaling based on first principles (filter time \propto BL¹) and (2) morphological models based on the measured allometries of engulfment capacity and baleen area (filter time \propto BL^{1.75}), and then tested these predictions with whale-borne tag data. Empirically, our results from the measured filter time (i.e. using tag data) (filter time \propto BL^{1.79}) show that the scaling of the feeding anatomy increases filtration time and results in a biomechanical constraint that affects foraging performance, as predicted. Consequently, the scaling of rorqual morphology predicts the allometry of foraging behavior and performance reasonably well with little deviation.

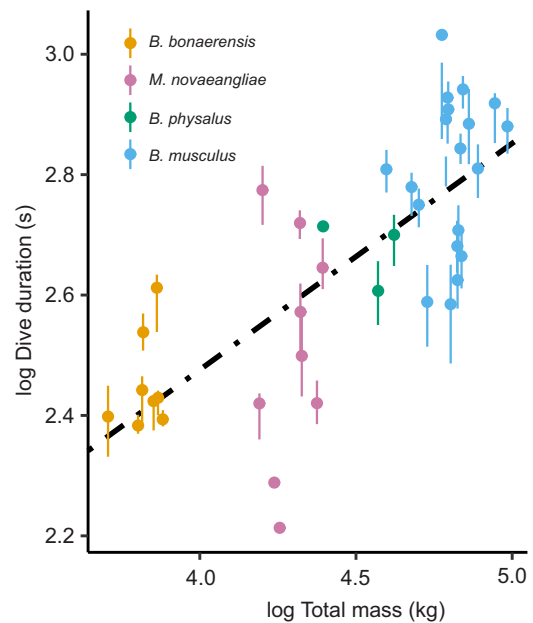


Fig. 4. Mean dive duration (s) increases with total body mass (kg). Nine minke whale deployments, three fin whale deployments, 21 blue whale deployments and nine humpback whale deployments were used in this analysis. The bars on each point represent the interquartile range (25–75%). Dashed line represents a general linear mixed model (slope=0.376; intercept=0.971; CI: 0.329–0.423).

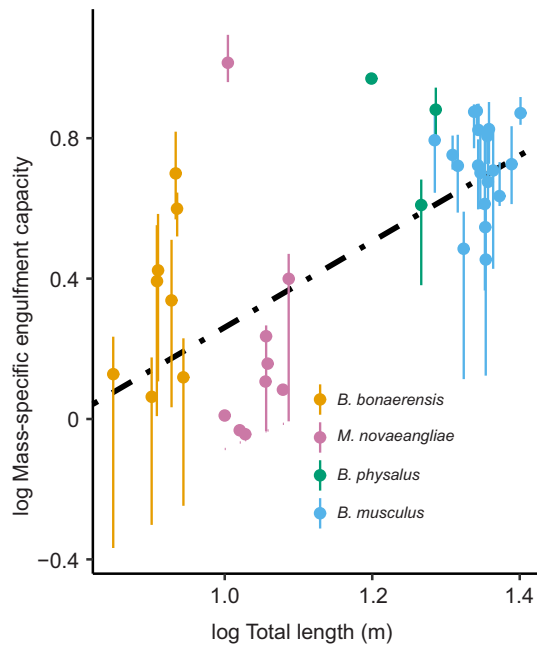


Fig. 5. Mean mass-specific engulfment capacity increases with total body length (m), measured using UAS imagery. Nine minke whale deployments, three fin whale deployments, 21 blue whale deployments and nine humpback whale deployments were used in this analysis. The bars on each point represent the interquartile range (25–75%). Dashed line represents a general linear mixed model (slope=1.22; intercept=-0.96; CI: 1.036–1.41).

Our results contrast with previous theories regarding filtration by large rorquals. Alexander (1998) posited that larger filter feeders may use a greater portion of the energy derived from their food intake to drive the filtration process than smaller filter feeders, but also suggested that this constraint could be ameliorated if filter area increased with positive allometry. Increasing filter area is effective for balaenids, such as bowhead whales (*Balaena mysticetus*) and right whales (*Eubalaena* spp.), whose baleen plates can reach lengths of 5 and 2 m, respectively (Werth, 2000). Balaenids swim slowly ($<1 \text{ m s}^{-1}$) through prey fields (Simon et al., 2009), using their long baleen plates with fine fringes to collect slow-moving copepods, and are able to stow these long plates because of complex jaw and skull adaptations (Werth, 2000). Although balaenid baleen area also exhibits negative allometry (balaenid baleen area $\propto \text{BL}^{1.47}$), balaenids have more baleen area per unit BL than rorquals (Werth et al., 2018).

Our study suggests that instead of increasing baleen area, rorquals have evolved relatively greater engulfment capacities to enhance overall energy intake. As a trade-off, larger whales spend more of their dive time filtering. A blue whale devotes 40% of its dive duration on average to filtration, whereas a minke whale only devotes an average of 21% of their dive duration to filtration (Table S2). If oxygen stores are isometric (oxygen stores $\propto \text{BM}^1$), the negative allometry of metabolic rate (metabolic rate $\propto \text{BM}^{0.66}$) suggests that dive capacity should increase with BM (dive capacity $\propto \text{BM}^{0.33}$) (Halsey et al., 2006; Noren and Williams, 2000). This prediction is generally confirmed with direct measures of diving behavior in both mammals and birds (dive capacity $\propto \text{BM}^{0.35}$) (Halsey et al., 2006). Our analyses of average dive duration from whale-borne tag data show that across species, larger rorqual whales with greater BM have longer dive durations, dive capacity $\propto \text{BM}^{0.38}$, which is very similar to the prediction of dive capacity $\propto \text{BM}^{0.35}$ from Halsey et al. (2006). Although this benefit of larger body size would seemingly allow animals to dive

deeper and lengthen their search for food (Doniol-Valcroze et al., 2011), thereby improving their foraging performance and fitness (Schoener, 1989), larger whales have devoted substantial proportions of their increased dive time to filtering engulfed water.

We interpreted the scaling of filter time in rorquals, a product of the allometry of the filter feeding apparatus, as a biomechanical constraint. If true, this constraint does not exist in isolation from rorqual foraging ecology. The relatively longer filter time (the biomechanical constraint) in larger rorquals shortens the time that could be spent searching for high-quality prey patches. Thus, if a whale lunges upon a patch that is small or not dense, it will result in less energetic gain per unit time. Given that lunge feeding is energetically costly, rorquals are reliant on hyper-dense prey patches proportionate in size to their engulfment capacity. Intense seasonal upwelling can facilitate these large prey swarms that allow rorquals to meet, and often exceed, their daily energetic demands (Goldbogen et al., 2019; Slater et al., 2017). Without these ideal patches, they face an ecological constraint that may negatively affect reproduction and survival (Goldbogen et al., 2019). However, if larger rorquals could modulate the volume engulfed in proportion to the size of the prey patch, the cost of a lunge would be reduced. Alternatively, rorquals may choose not to forage on small, low-quality prey patches and instead search for higher quality prey fields at other locations.

Large whales, such as blue and fin whales, often forage in the open ocean along edges of canyons, where space is not limiting and krill can aggregate in large patches or layers (Genin, 2004). Although larger rorquals lunge less frequently, their enormous engulfment capacity leads to more water processed per dive, both in absolute and mass-specific terms (Fig. 5). This mechanistic explanation, wherein the amount of prey consumed per dive increases with increasing engulfment capacity, ameliorates the physiological and biomechanical constraint of longer filter time and allows for the evolution of gigantism in this lineage (Goldbogen et al., 2019). This high-efficiency foraging is critical for rorquals to support the energetic demands of extreme size, as well as to account for reduced feeding efforts during migration and reproduction. The mitigation of the biomechanical constraint is dependent upon the presence of incredibly vast yet ephemeral prey patches. If dense, high-quality prey is not limiting, larger whales will engulf more krill than smaller whales with each lunge (Fig. 5), circumventing the ecological constraint.

We sought to determine the maximum number of lunges executed per dive as this count may reflect a physiological limit given optimal prey density and distribution (Friedlaender et al., 2016; Goldbogen et al., 2012; Hazen et al., 2015). In presumably optimal foraging conditions, maximum lunge count per dive in minke whales (18) was twice that of much larger fin whales (9) and higher than the blue whales (11) (Table 2). Although we excluded lunges that occurred at depths shallower than 50 m in our analysis, a tagged minke whale in our records performed 22 lunges per dive, albeit at 40 m. Even greater lunge rates were recorded by Friedlaender et al. (2014), who recorded a minke whale lunging 24 times per dive. These details highlight the complexity of explaining lunge rate without concomitant prey data. While lunge count is definitively influenced by body size, other factors such as prey density and prey type contribute to the choice of when and where to perform a high-cost, high-yield maneuver (Friedlaender et al., 2019; Goldbogen et al., 2015). Although we only compared foraging rates of krill-feeding rorquals, some rorqual species also exploit other patchy prey like forage fish. We would expect the lunge count per dive, dive duration, and mean dive depth to vary based on the behavior of the fish school. Fish behavior drives the lunge rates and other variables more than oxygen and physiological limitations (Cade et al., 2020).

Nevertheless, our results on size-dependent performance may reflect how different sized rorquals have evolved prey preferences, broadly defined. Smaller body size and smaller gulps lead to less prey intake per unit effort. However, smaller size provides the flexibility needed to hunt in complex environments and upon smaller or unevenly distributed prey patches to satisfy relatively lower energetic needs. The biomechanical constraint is present, but does not compound the ecological constraint for small rorquals. In contrast, the increased filter time of larger rorquals curtails foraging performance by decreasing lunge count per dive, but because of extraordinary engulfment capacity, larger rorquals can collect more prey per unit body mass during a dive. The biomechanical constraint becomes increasingly limiting for larger rorquals, and if a large rorqual cannot find a high-density prey patch, they ultimately face an ecological constraint. The smaller rorquals, such as minke, are less constrained by both their environment and biomechanics, and therefore may be similarly less limited in terms of prey preference and ecological niche. Accordingly, rorquals appear to trade off body size and protection from predation (Ford and Reeves, 2008) for variable habitats and prey distribution flexibility. In a changing environment that may disrupt trophic linkages and the formation of prey patches (Fleming et al., 2016), larger, prey-specialist whales may be more susceptible to changes in these distributions, given that they must focus foraging efforts on only a few select feeding events.

Acknowledgements

The authors thank the boat crew of the John Martin (Moss Landing Marine Labs) and the Cascadia Research crew for their assistance in the data collection. We also thank Dr Nikolai Liebsch and Dr Peter Kraft from Customized Animal Tracking Solutions for their continued work with our group. Finally, we thank William K. Oestreich, Max F. Czapanskiy, Mark W. Denny, Elliot L. Hazen and Stuart H. Thompson for their invaluable comments and feedback on this manuscript.

Competing interests

The authors declare no competing or financial interests.

Author contributions

Conceptualization: S.R.K., M.S.S., D.E.C., J.A.G.; Methodology: S.R.K., M.S.S., D.E.C., K.C.B.; Software: D.E.C., K.C.B., J.A.F.; Validation: S.R.K., M.S.S., D.E.C., P.S.S.; Formal analysis: S.R.K., M.S.S., D.E.C., P.S.S., K.C.B., J.D., J.A.F.; Investigation: S.R.K., M.S.S., D.E.C., P.S.S., K.C.B., J.A.C., J.D., J.A.F., A.S.F., D.W.J., A.J.W., J.A.G.; Resources: K.C.B., J.A.C., J.D., D.W.J., A.J.W., J.A.G.; Data curation: S.R.K., M.S.S., D.E.C., P.S.S., K.C.B., J.D., J.A.F., A.J.W.; Writing - original draft: S.R.K., J.A.G.; Writing - review & editing: S.R.K., M.S.S., D.E.C., P.S.S., K.C.B., J.D., J.A.F., A.S.F., D.W.J., A.J.W., J.A.G.; Visualization: S.R.K., M.S.S.; Supervision: J.A.C., A.S.F., D.W.J., J.A.G.; Project administration: J.A.C., A.S.F., D.W.J., J.A.G.; Funding acquisition: J.A.C., A.S.F., D.W.J., J.A.G.

Funding

This research was funded in part by grants from the National Science Foundation (IOS-1656691, IOS-1656676, IOS-1656656, OPP-1644209) and the Office of Naval Research (N000141612477), and a Terman Fellowship from Stanford University. Additional Monterey Bay CATS tag deployments were funded by grants from the American Cetacean Society Monterey and San Francisco Bay chapters, and by the Drs Earl H. Myers and Ethel M. Myers Oceanographic and Marine Biology Trust.

Data availability

The datasets supporting this article are available at Kahane-Rapport et al. (2020): [dryad.n5tb2rbt2](https://doi.org/10.1242/jeb.224196).

Supplementary information

Supplementary information available online at <https://jeb.biologists.org/lookup/doi/10.1242/jeb.224196.supplemental>

References

Alexander, R. M. (1998). All-time giants: the largest animals and their problems. *Palaeontology* **41**, 1231-1245.
Bates, D., Mächler, M., Bolker, B. and Walker, S. (2015). Fitting linear mixed-effects models using lme4. *J. Stat. Software* **67**, 1-48. doi:10.18637/jss.v067.i01

Bird, C. N. and Bierlich, K. C. (2020). CollatR: A GUI to collate MorphoMetriX outputs. *J. Open Source Soft.* **5**, 2328. doi:10.21105/joss.02328
Cade, D. E., Friedlaender, A. S., Calambokidis, J. and Goldbogen, J. A. (2016). Kinematic diversity in rorqual whale feeding mechanisms. *Curr. Biol.* **26**, 2617-2624. doi:10.1016/j.cub.2016.07.037
Cade, D. E., Barr, K. R., Calambokidis, J., Friedlaender, A. S. and Goldbogen, J. A. (2018). Determining forward speed from accelerometer jiggle in aquatic environments. *J. Exp. Biol.* **221**, jeb170449. doi:10.1242/jeb.170449
Cade, D. E., Carey, N., Domenici, P., Potvin, J. and Goldbogen, J. A. (2020). Predator-informed looming stimulus experiments reveal how large filter feeding whales capture highly maneuverable forage fish. *Proc. Natl. Acad. Sci. USA* **117**, 472-478. doi:10.1073/pnas.1911099116
Calder, W. A. (1984). *Size, Function, and Life History*. Cambridge, MA: Harvard University Press.
Carrier, D. R. (1994). Ontogeny of jumping performance in the black-tailed jackrabbit (*Lepus californicus*). *Zool. Anal. Complex Syst.* **98**, 309-313.
Clauzet, A. (2013). How large should whales be? *PLoS ONE* **8**, e53967. doi:10.1371/journal.pone.0053967
Domenici, P. (2001). The scaling of locomotor performance in predator-prey encounters: from fish to killer whales. *Comp. Biochem. Physiol. A Mol. Integr. Physiol.* **131**, 169-182. doi:10.1016/S1095-6433(01)00465-2
Doniol-Valcroze, T., Lesage, V., Giard, J. and Michaud, R. (2011). Optimal foraging theory predicts diving and feeding strategies of the largest marine predator. *Behav. Ecol.* **22**, 880-888. doi:10.1093/beheco/arr038
Durban, J. W., Moore, M. J., Chiang, G., Hickmott, L. S., Boccoicelli, A., Howes, G., Bahamonde, P. A., Perryman, W. L. and LeRoi, D. J. (2016). Photogrammetry of blue whales with an unmanned hexacopter. *Mar. Mamm. Sci.* **32**, 1510-1515. doi:10.1111/mms.12328
Fleming, A. H., Clark, C. T., Calambokidis, J. and Barlow, J. (2016). Humpback whale diets respond to variance in ocean climate and ecosystem conditions in the California Current. *Glob. Chang. Biol.* **22**, 1214-1224. doi:10.1111/gcb.13171
Ford, J. K. B. and Reeves, R. R. (2008). Fight or flight: antipredator strategies of baleen whales. *Mamm. Rev.* **38**, 50-86. doi:10.1111/j.1365-2907.2008.00118.x
Friedlaender, A. S., Goldbogen, J. A., Nowacek, D. P., Read, A. J., Johnston, D. and Gales, N. (2014). Feeding rates and under-ice foraging strategies of the smallest lunge filter feeder, the Antarctic minke whale (*Balaenoptera bonaerensis*). *J. Exp. Biol.* **217**, 2851-2854. doi:10.1242/jeb.106682
Friedlaender, A. S., Johnston, D. W., Tyson, R. B., Kaltenberg, A., Goldbogen, J. A., Stimpert, A. K., Curtice, C., Hazen, E. L., Halpin, P. N., Read, A. J. et al. (2016). Multiple-stage decisions in a marine central-place forager. *R. Soc. Open Sci.* **3**, 160043. doi:10.1098/rsos.160043
Friedlaender, A. S., Bowers, M. T., Cade, D., Hazen, E. L., Stimpert, A. K., Allen, A. N., Calambokidis, J., Fahlbusch, J., Segre, P., Visser, F. et al. (2019). The advantages of diving deep: fin whales quadruple their energy intake when targeting deep krill patches. *Funct. Ecol.* **34**, 497-506. doi:10.1111/1365-2435.13471
Friedman, M., Shimada, K., Martin, L. D., Everhart, M. J., Liston, J., Maltese, A., Triebold, M. (2010). 100-million-year dynasty of giant planktivorous bony fishes in the Mesozoic seas. *Science* **327**, 990-993. doi:10.1126/science.1184743
Galilei, G. (1914). Dialogues concerning two new sciences (translated from Italian and Latin by Henry Crew and Alfonso de Salvio). New York. <https://oll.libertyfund.org/titles/753>
Genin, A. (2004). Bio-physical coupling in the formation of zooplankton and fish aggregations over abrupt topographies. *J. Mar. Syst.* **50**, 3-20. doi:10.1016/j.jmarsys.2003.10.008
Goldbogen, J. A., Pyenson, N. D. and Shadwick, R. E. (2007). Big gulps require high drag for fin whale lunge feeding. *Mar. Ecol. Prog. Ser.* **349**, 289-301. doi:10.3354/meps07066
Goldbogen, J. A., Potvin, J. and Shadwick, R. E. (2010). Skull and buccal cavity allometry increase mass-specific engulfment capacity in fin whales. *Proc. Biol. Sci.* **277**, 861-868. doi:10.1098/rspb.2009.1680
Goldbogen, J. A., Calambokidis, J., Oleson, E., Potvin, J., Pyenson, N. D., Schorr, G. and Shadwick, R. E. (2011). Mechanics, hydrodynamics and energetics of blue whale lunge feeding: efficiency dependence on krill density. *J. Exp. Biol.* **214**, 131-146. doi:10.1242/jeb.048157
Goldbogen, J. A., Calambokidis, J., Croll, D. A., McKenna, M. F., Oleson, E., Potvin, J., Pyenson, N. D., Schorr, G., Shadwick, R. E. and Tershy, B. R. (2012). Scaling of lunge-feeding performance in rorqual whales: mass-specific energy expenditure increases with body size and progressively limits diving capacity. *Funct. Ecol.* **26**, 216-226. doi:10.1111/j.1365-2435.2011.01905.x
Goldbogen, J. A., Hazen, E. L., Friedlaender, A. S., Calambokidis, J., DeRuiter, S. L., Stimpert, A. K. and Southall, B. L. (2015). Prey density and distribution drive the three-dimensional foraging strategies of the largest filter feeder. *Funct. Ecol.* **29**, 951-961. doi:10.1111/1365-2435.12395
Goldbogen, J. A., Cade, D. E., Calambokidis, J., Friedlaender, A. S., Potvin, J., Segre, P. S. and Werth, A. J. (2017). How baleen whales feed: the biomechanics of engulfment and filtration. *Ann. Rev. Mar. Sci.* **9**, 367-386. doi:10.1146/annurev-marine-122414-033905
Goldbogen, J. A., Cade, D. E., Wisniewska, D. M., Potvin, J., Segre, P. S., Savoca, M. S., Hazen, E. L., Czapanskiy, M. F., Kahane-Rapport, S. R. and

- DeRuiter, S. L. et al.** (2019). Why whales are big but not bigger: physiological drivers and ecological limits in the age of ocean giants. *Science* **366**, 1367-1372. doi:10.1126/science.aax9044
- Hadfield, J. D.** (2010). MCMC methods for multi-response generalized linear mixed models: the MCMCglmm R package. *J. Stat. Software* **33**, 1-22. doi:10.18637/jss.v033.i02
- Haldane, J. B. S.** (1926). On being the right size. *Harper Mag.* **152**, 424-427.
- Halsey, L. G., Butler, P. J. and Blackburn, T. M.** (2006). A phylogenetic analysis of the allometry of diving. *Am. Nat.* **167**, 276-287. doi:10.1086/499439
- Hazen, E. L., Friedlaender, A. S. and Goldbogen, J. A.** (2015). Blue whales (*Balaenoptera musculus*) optimize foraging efficiency by balancing oxygen use and energy gain as a function of prey density. *Sci. Adv.* **1**, e1500469. doi:10.1126/sciadv.1500469
- Hespenheide, H. A.** (1973). Ecological inferences from morphological data. *Annu. Rev. Ecol. Syst.* **4**, 213-229. doi:10.1146/annurev.es.04.110173.001241
- Hirt, M. R., Jetz, W., Rall, B. C. and Brose, U.** (2017). A general scaling law reveals why the largest animals are not the fastest. *Nat. Ecol. Evol.* **1**, 1116-1122. doi:10.1038/s41559-017-0241-4
- Holliday, R.** (2005). Ageing and the extinction of large animals. *Biogerontology* **6**, 151-156. doi:10.1007/s10522-005-3458-6
- Irving, L.** (1973). Aquatic mammals. In *Comparative Physiology of Thermoregulation: Special Aspects of Thermoregulation* (ed. G. C. Whitton), pp. 47-96. Academic Press.
- Johnson, M. P. and Tyack, P. L.** (2003). A digital acoustic recording tag for measuring the response of wild marine mammals to sound. *IEEE J. Oceanic Eng.* **28**, 3-12. doi:10.1109/JOE.2002.808212
- Kahane-Rappoport, S. R.** (2020). Data set for 'Lunge filter feeding biomechanics constrain rorqual foraging ecology across scale', v3, Stanford University. *Dryad Dataset* doi:10.5061/dryad.n5tb2rbt2.
- Kahane-Rappoport, S. R. and Goldbogen, J. A.** (2018). Allometric scaling of morphology and engulfment capacity in rorqual whales. *J. Morphol.* **279**, 1256-1268. doi:10.1002/jmor.208
- Kawamura, A.** (1974). Food and feeding ecology in the Southern Sei whale. *Sci. Rep. Whales Res. Inst.* **26**, 25-144.
- Kelt, D. A. and Van Vuren, D.** (1999). Energetic constraints and the relationship between body size and home range area in mammals. *Ecology* **80**, 337-340. doi:10.1890/0012-9658(1999)080[0337:ECATRB]2.0.CO;2
- Kerkhoff, A. J. and Enquist, B. J.** (2009). Multiplicative by nature: why logarithmic transformation is necessary in allometry. *J. Theor. Biol.* **257**, 519-521. doi:10.1016/j.jtbi.2008.12.026
- LaBarbera, M.** (1984). Feeding currents and particle capture mechanisms in suspension feeding animals. *Am. Zool.* **24**, 71-84.
- Mackintosh, N. A.** (1929). Southern blue and fin whales. *Discov. Rep.* **1**, 257-540.
- Mackintosh, N. A.** (1942). The southern stocks of whalebone whales. *Discov. Rep.* **22**, 197-300.
- Matthews, L. H.** (1937). The humpback whale, *Megaptera nodosa*. *Discov. Rep.* **17**, 7-92.
- Matthews, L. H.** (1938). *The Sei Whale, Balaenoptera borealis*. Cambridge University Press.
- Noren, S. R. and Williams, T. M.** (2000). Body size and skeletal muscle myoglobin of cetaceans: adaptations for maximizing dive duration. *Comp. Biochem. Physiol. A Mol. Integr. Physiol.* **126**, 181-191. doi:10.1016/S1095-6433(00)00182-3
- Paladino, F. V., O'Connor, M. P. and Spotila, J. R.** (1990). Metabolism of leatherback turtles, gigantothermy, and thermoregulation of dinosaurs. *Nature* **344**, 858-860. doi:10.1038/344858a0
- Peters, R. H.** (1983). Physiological correlates of size. In *The Ecological Implications of Body Size*, pp. 45-53. Cambridge University Press.
- Potvin, J., Goldbogen, J. A. and Shadwick, R. E.** (2009). Passive versus active engulfment: verdict from trajectory simulations of lunge-feeding fin whales *Balaenoptera physalus*. *J. R. Soc. Interface* **6**, 1005-1025. doi:10.1098/rsif.2008.0492
- Potvin, J., Goldbogen, J. A. and Shadwick, R. E.** (2012). Metabolic expenditures of lunge feeding rorquals across scale: implications for the evolution of filter feeding and the limits to maximum body size. *PLoS ONE* **7**, e44854. doi:10.1371/journal.pone.0044854
- Schmidt-Nielsen, K.** (1984). *Scaling: Why is Animal Size so Important?* Cambridge University Press.
- Schoener, T. W.** (1989). How feeding relations affect body size - a citation classic commentary on models of optimal size for solitary predators by Schoener, T.W. *Curr. Contents Agric. Biol. Environ. Sci.* **38**, 14.
- Scholander, P. F., Hock, R., Walters, V. and Irving, L.** (1950). Adaptation to cold in Arctic and Tropical mammals and birds in relation to body temperature, insulation, and basal metabolic rate. *Biol. Bull.* **99**, 259-271. doi:10.2307/1538742
- Sebens, K. P.** (1982). The limits to indeterminate growth: an optimal size model applied to passive suspension feeders. *Ecology* **63**, 209-222. doi:10.2307/1937045
- Simon, M., Johnson, M., Tyack, P. and Madsen, P. T.** (2009). Behaviour and kinematics of continuous ram filtration in bowhead whales (*Balaena mysticetus*). *Proc. R. Soc. B Biol. Sci.* **276**, 3819-3828. doi:10.1098/rspb.2009.1135
- Simon, M., Johnson, M. and Madsen, P. T.** (2012). Keeping momentum with a mouthful of water: behavior and kinematics of humpback whale lunge feeding. *J. Exp. Biol.* **215**, 3786-3798. doi:10.1242/jeb.071092
- Slater, G. J., Goldbogen, J. A. and Pyenson, N. D.** (2017). Independent evolution of baleen whale gigantism linked to Plio-Pleistocene ocean dynamics. *Proc. Biol. Sci.* **284**, 20170546. doi:10.1098/rspb.2017.0546
- Smith, F. A., Elliott Smith, R. E., Lyons, S. K. and Payne, J. L.** (2018). Body size downgrading of mammals over the late Quaternary. *Science* **360**, 310-313. doi:10.1126/science.aao5987
- Taylor, C. R., Heglund, N. C., McMahon, T. A. and Looney, T. R.** (1980). Energetic cost of generating muscular force during running: a comparison of large and small animals. *J. Exp. Biol.* **86**, 9-18.
- Torres, W. and Bierlich, K.** (2020). MorphoMetriX: a photogrammetric measurement GUI for morphometric analysis of megafauna. *J. Open Sour. Software* **5**, 1825. doi:10.21105/joss.01825
- Vermeij, G. J.** (2016). Gigantism and its implications for the history of life. *PLoS ONE* **11**, e0146092. doi:10.1371/journal.pone.0146092
- Werth, A. J.** (2000). Feeding in marine mammals. In *Feeding: Form, Function, and Evolution in Tetrapod Vertebrates* (ed. K. Schwenk), pp. 487-526. Academic Press.
- Werth, A. J., Potvin, J., Shadwick, R. E., Jensen, M. M., Cade, D. E. and Goldbogen, J. A.** (2018). Filtration area scaling and evolution in mysticetes: trophic niche partitioning and the curious cases of sei and pygmy right whales. *Biol. J. Linn. Soc.* **20**, 264-279. doi:10.1093/biolinnean/bly121
- White, C. R. and Kearney, M. R.** (2014). Metabolic scaling in animals: methods, empirical results, and theoretical explanations. *Compr. Physiol.* **4**, 231-256. doi:10.1002/cphy.c110049
- Wiedenmann, J., Cresswell, K. A., Goldbogen, J., Potvin, J. and Mangel, M.** (2011). Exploring the effects of reductions in krill biomass in the Southern Ocean on blue whales using a state-dependent foraging model. *Ecol. Model.* **222**, 3366-3379. doi:10.1016/j.ecolmodel.2011.07.013